

Fire radiative
impacts

J. C. Péré et al.

This discussion paper is/has been under review for the journal Atmospheric Chemistry and Physics (ACP). Please refer to the corresponding final paper in ACP if available.

Direct radiative effect of the Russian wildfires and their impact on air temperature and atmospheric dynamics during August 2010

J. C. Péré¹, B. Bessagnet², M. Mallet³, F. Waquet¹, I. Chiapello¹, F. Minvielle¹, V. Pont³, and L. Menut⁴

¹Laboratoire d'Optique Atmosphérique, Université Lille 1 CNRS/UMR8518, 59655 Villeneuve d'Ascq, France

²Institut National de l'Environnement Industriel et des Risques, Parc Technologique Alata, 60550 Verneuil en Halatte, France

³Laboratoire d'Aérodologie, Observatoire Midi-Pyrénées, Université Paul Sabatier UMR/CNRS 5560, 14 Avenue Edouard Belin, 31400 Toulouse, France

⁴Laboratoire de Météorologie Dynamique, Ecole Polytechnique UMR/CNRS 8539, 91128 Palaiseau, France

Title Page

Abstract

Introduction

Conclusions

References

Tables

Figures

◀

▶

◀

▶

Back

Close

Full Screen / Esc

Printer-friendly Version

Interactive Discussion



Received: 15 May 2013 – Accepted: 3 June 2013 – Published: 14 June 2013

Correspondence to: J. C. Péré (jean-christophe.pere@univ-lille1.fr)

Published by Copernicus Publications on behalf of the European Geosciences Union.

ACPD

13, 15829–15866, 2013

**Fire radiative
impacts**

J. C. Péré et al.

Title Page

Abstract

Introduction

Conclusions

References

Tables

Figures

⏪

⏩

◀

▶

Back

Close

Full Screen / Esc

Printer-friendly Version

Interactive Discussion



Abstract

The present study aims at investigating the shortwave aerosol direct radiative forcing (ADRF) and its feedback on air temperature and atmospheric dynamics during a major fire event that occurred in Russia during August 2010. The methodology is based on an off-line coupling between the CHIMERE chemistry-transport and the Weather Research and Forecasting (WRF) models. First, simulations for the period 5–12 August 2010 have been evaluated by using AERONET and satellite measurements of the POLarization and Directionality of the Earth's Reflectance (POLDER) and the Cloud-Aerosol Lidar with Orthogonal Polarization (CALIOP) sensors. During this period, elevated POLDER AOT are found over a large part of Eastern Europe with values above 2 (at 550 nm) in the aerosol plume. According to CALIOP observations, particles remain confined within the first five kilometres of the atmospheric layer. Comparisons with satellite measurements show the ability of CHIMERE to reproduce the regional and vertical distribution of aerosols during their transport from the source region. Over Moscow, AERONET measurements indicate an important increase of AOT (340 nm) from 0.7 on 5 August to 2–4 between 6 and 10 August when the aerosol plume is advected over the city. Particles are mainly observed in the fine size mode (radius in the range 0.2–0.4 μm) and are characterized by elevated SSA (0.95–0.96 between 440 and 1020 nm). Also, comparisons of simulations with AERONET measurements show that aerosol physical-optical properties (size distribution, AOT, SSA) have been well simulated over Moscow in term of intensity and/or spectral dependence. Secondly, modelled aerosol optical properties have been used as input in the radiative transfer code of WRF to evaluate their direct radiative impact. Simulations indicate a significant reduction of solar radiation at the ground (up to 80–150 Wm^{-2} in diurnal-averaged) over a large part of Eastern Europe due to the presence of the aerosol plume. This ADRF causes an important reduction of the near-surface air temperature between 0.2 and 2.6 $^{\circ}\text{C}$ at a regional scale. Moscow has been also affected by the aerosol plume, especially between 6 and 10 August. During this period, aerosol causes a significant

Fire radiative impacts

J. C. Péré et al.

Title Page

Abstract

Introduction

Conclusions

References

Tables

Figures

◀

▶

◀

▶

Back

Close

Full Screen / Esc

Printer-friendly Version

Interactive Discussion



Fire radiative impacts

J. C. Péré et al.

Title Page

Abstract

Introduction

Conclusions

References

Tables

Figures

◀

▶

◀

▶

Back

Close

Full Screen / Esc

Printer-friendly Version

Interactive Discussion



reduction of surface shortwave radiation (up to 70–84 W m⁻² in diurnal-averaged) with a moderate part (20–30 %) due to solar absorption within the aerosol layer. The resulting feedbacks lead to a cooling of the air up to 1.6 °C at the surface and 0.1 °C at an altitude of 1500–2000 m (in diurnal-averaged), that contribute to stabilize the atmospheric boundary layer (ABL). Indeed, a reduction of the ABL height of 13 to 65 % have been simulated during daytime in presence of aerosols. This decrease is the result of a lower air entrainment as the vertical wind speed in the ABL is shown to be reduced by 5 to 80 % (at midday) when the feedback of the ADRF is taken into account. In turn, CHIMERE simulations driven by the WRF meteorological fields including this ADRF feedback result in a large increase in the modeled near-surface PM₁₀ concentrations (up to 99 %) due to their lower vertical dilution in the ABL, which tend to reduce model biases with the ground PM₁₀ values observed over Moscow during this specific period.

1 Introduction

It is now well recognized that biomass burning aerosols can affect the earth's radiative balance by interacting with solar radiation. Their scattering (organic carbon) and absorbing (black and brown carbon) components can result either in a negative or positive shortwave direct radiative forcing with some potential influence on the regional climate, especially during important fire activities (Forster et al., 2007). Recent studies dealt with the regional climate impact of aerosols over areas affected by biomass burning episodes such as southern and western Africa (Tummon et al., 2011; Malavelle et al., 2011), Amazonia (Zhang et al., 2009) or Indonesia (Ott et al., 2010) and highlighted the complexity of these impacts such as changes in the atmospheric dynamics, precipitation regime and temperature gradient. Although the global fire activity is expected to increase in a future warmer climate (Moritz et al., 2012), the radiative effects of smoke aerosols on the atmosphere still remain uncertain (Carslaw et al., 2010), because of uncertainties in the amount of biomass burning aerosols emitted, their transport and

vertical distribution and the characterisation of their microphysical and optical properties.

During mid-July to mid-August 2010, the western part of Russia was affected by a strong heatwave episode favourable to the development of numerous wildfires (Witte et al., 2011). During this period, the release of smoke particles in the atmosphere associated with the accumulation of urban/industrial pollution largely contributed to high levels of aerosol concentrations over the Moscow region with daily PM₁₀ values up to 700 µg m⁻³ (Konovalov et al., 2011). Recently, Chubarova et al. (2012) analysed the optical and radiative properties of particles during this specific fire event by using ground measurements at Moscow and Zvenigorod. They recorded elevated aerosol loadings over these two locations that induced an important direct radiative forcing reaching, on 7 August 2010, the instantaneous value -167 W m^{-2} (at midday) at the top of the atmosphere, corresponding to an aerosol optical thickness of 6.4 at 500 nm. This intense aerosol radiative forcing is expected to have some potential feedbacks on the regional climate. However, the climatic impact of aerosols at regional scale during this intense biomass burning episode has not yet been investigated.

In this context, the present modelling study aims at analysing the chemical and optical properties of aerosols, their shortwave direct radiative forcing and its feedback on air temperature and atmospheric dynamics during the peak of fire activity that occurred during the first part of August 2010 over Eastern Europe. This work is based on an off-line coupling between the CHIMERE chemistry-transport (Menut et al., 2013) and the WRF meteorological (Skamarock et al., 2001) models. An advantage of such methodology is the use of two sophisticated meso-scale models with reasonable computation time. Section 2 describes the configuration of each model and their off-line coupling. Then, a description and evaluation of the modelled microphysical and optical properties of particles are given (Sect. 3.1) and their impacts on shortwave solar fluxes, temperature profile and atmospheric dynamics are discussed (Sect. 3.2). Finally, conclusions are made in Sect. 4.

Fire radiative impacts

J. C. Péré et al.

Title Page

Abstract

Introduction

Conclusions

References

Tables

Figures

◀

▶

◀

▶

Back

Close

Full Screen / Esc

Printer-friendly Version

Interactive Discussion



2 Methodology

2.1 Description of the CHIMERE model

CHIMERE is a 3-D chemistry-transport model developed to simulate gaseous and particulate chemistry at regional scale (Bessagnet et al., 2004; Menut et al., 2013). In this study, the horizontal grid ranges from 43.40 to 63.20° N in latitude and from 18.70 to 57.30° E in longitude with a 30 km resolution and the vertical grid includes 15 levels from surface to 500 hPa. The aerosol module takes into account 9 species (sulphate, nitrate, ammonium, primary organic (OC) and black carbon (BC), secondary organic aerosols (SOA), sea salt, dust and water) distributed within 8 bins ranging from 40 nm to 10 µm (in diameter). Dynamical processes influencing aerosol population such as nucleation of sulphuric acid, coagulation, adsorption/desorption, wet and dry deposition and scavenging are taken into account. Particles can be scavenged either by coagulation with cloud droplets or by precipitating drops.

Anthropogenic emissions of gaseous and particulate origin are taken from EMEP inventory and soil dust are produced within the domain according to the parametrization of Vautard et al. (2005). Carbonaceous emissions from fossil fuel and biofuel consumption are issued from the work of Junker and Liousse (2008). The formation of SOA is represented according to oxidation of relevant precursors and gas particle partitioning of the condensable oxidation products. This specific chemical scheme includes precursors of biogenic (such as isoprene, terpene, etc.) and anthropogenic (such as benzene, toluene, etc.) origin. Precursors emitted by vegetation are calculated using the Model of Emissions of Gases and Aerosols from Nature (MEGAN) (Guenther et al., 2006) scheme. The gas-particle partitioning formulation of Pun et al. (2006) has been adapted to the SOA formation mechanism implemented in CHIMERE (Bessagnet et al., 2009).

The important release of aerosols and gases by wildfires that affected Russia during summer 2010 are taken into account according to the work of Kaiser et al. (2012). In their methodology, biomass burning emissions are calculated with the Global Fire As-

Fire radiative impacts

J. C. Péré et al.

[Title Page](#)[Abstract](#)[Introduction](#)[Conclusions](#)[References](#)[Tables](#)[Figures](#)[◀](#)[▶](#)[◀](#)[▶](#)[Back](#)[Close](#)[Full Screen / Esc](#)[Printer-friendly Version](#)[Interactive Discussion](#)

Fire radiative impacts

J. C. Péré et al.

Title Page

Abstract

Introduction

Conclusions

References

Tables

Figures

◀

▶

◀

▶

Back

Close

Full Screen / Esc

Printer-friendly Version

Interactive Discussion



simulation System by assimilating Fire Radiative Power observations from the Moderate Resolution Imaging Spectroradiometer (MODIS) spatial instrument. The combustion rate is evaluated with specific land-cover conversion factors and emission factors for 40 gaseous and aerosol species from current literature are used. These fire emissions combined with the Monitoring Atmospheric Composition and Change aerosol model have been shown to well capture the Russian fire plume during summer 2010 (Kaiser et al., 2012).

Optical properties of particles are required to evaluate their direct radiative impact. A description of the scheme designed to calculate aerosol optical properties from concentrations, size distribution and chemical composition simulated by CHIMERE is reported by Péré et al. (2010). In the present study, Aerosol Optical Thickness (AOT), Single Scattering Albedo (SSA) and asymmetry parameter (g) are evaluated using Mie theory for a core-shell aerosol mixing in which each particle is composed by a core of primary organics, black carbon and mineral dust surrounded by a shell of secondary species (sulphate, nitrate, ammonium, SOA), sea salt and water. This optical treatment has been shown to well reproduce aerosol optical properties compared to pure external or internally homogeneous mixing (Péré et al., 2009).

2.2 Description of the WRF model and its off-line coupling with CHIMERE

The version 3.1 of WRF (Skamarock et al., 2001) has been used for a domain covering Eastern Europe with the same horizontal resolution as CHIMERE (30 km) and including 27 vertical levels (from 40 m to about 20 km). The configuration used here is the same as in Péré et al. (2011) and includes the WRF single-moment five-class scheme of Hong et al. (2006) for the microphysics module, the Kain–Fritsch cumulus parametrization (Kain, 2004), the NOAH land surface module of Chen and Dudhia (2001) and the Yonsei University planetary boundary layer scheme (Hong et al., 2006; Hong, 2007). It should be noted that interactions between aerosols and clouds (such as activation of particles in cloud condensation nuclei) are not explicitly resolved in this configuration of WRF. Within the atmosphere, radiation responds to clouds and water

Fire radiative impacts

J. C. Péré et al.

Title Page

Abstract

Introduction

Conclusions

References

Tables

Figures

◀

▶

◀

▶

Back

Close

Full Screen / Esc

Printer-friendly Version

Interactive Discussion



vapour distribution, carbon dioxide, ozone and trace gases as well as the presence of aerosols through an off-line coupling with the CHIMERE model. For shortwave radiation, the Goddard model (Chou and Suarez, 1994) including 11 spectral bands from 0.2 to 6 μm is used, while for longwave radiation, the Rapid Radiative Transfer model (RRTM) (Mlawer et al., 1997) including 16 spectral bands from 6 to 1000 μm has been chosen. It should be noted that aerosol impacts on longwave radiation, such as sea salt and mineral dust, are not taken into account in RRTM in this version of WRF.

In this study, an off-line and one-way coupling between CHIMERE and WRF has been performed. A detailed description and evaluation of this methodology can be found in Péré et al. (2011). Meteorological input parameters required by CHIMERE such as 3-D wind, air temperature or relative humidity are provided by WRF. Secondly, aerosol optical properties (AOT, SSA, and g) are simulated using CHIMERE for an aerosol core-shell mixing. Finally, meteorological simulations are performed using aerosol optical properties as inputs in the WRF radiative transfer module. Here we focus our study on the impact of fine aerosols ($10 \text{ nm} \leq \text{radius} \leq 5 \mu\text{m}$) on shortwave solar radiation. To reduce computing time, aerosol optical properties are calculated at 4 four wavelengths (0.3, 0.4, 0.6 and 0.99 μm) and then interpolated on the shortwave radiation bands (0.2–6 μm) of the WRF radiative transfer module. The wavelength-dependent refractive indexes of each chemical species used to perform Mie calculations are reported in Table 1. AOT, SSA and g are estimated for the 15 vertical layers of the CHIMERE model ranging from 40 m to about 6 km a.g.l. For higher altitude, a climatology of optical properties for the free troposphere and the stratosphere (Hess et al., 1998) has been used (Table 2). To estimate the shortwave ADRF and its feedback on air temperature and atmospheric dynamics, two simulations have been performed for the period 5–12 August 2010: one including the ADRF and the other without. It should be noted that this methodology enables only the investigation of climate feedbacks due to the ADRF. The indirect effect is not treated in the present study as it would require a complete on-line and two-way coupling between WRF and CHIMERE.

3 Results and discussions

3.1 Evaluation of the modelled aerosol optical properties

Simulations of aerosol properties during this specific episode have been evaluated with POLDER, CALIOP and AERONET observations. POLDER is on-board the PARASOL satellite of the A-Train constellation launched in December 2004. This sensor is a wide field of view imaging radiometer providing spectral, directional and polarized radiance measurements over land and ocean for visible wavelengths with a local overpass time around 10.30 a.m. over Europe. In this study, level-2 cloud-free AOT data at 550 nm with a 18 km horizontal resolution and corresponding to fine aerosols (radius less than 0.3 μm) have been used (Deuzé et al., 2001; Tanré et al., 2011). The CALIOP instrument, on-board the CALIPSO satellite of the A-Train platform since April 2006, is an elastic backscatter lidar providing the vertical distribution of aerosols and clouds. Here, we use the level-2 product of the aerosol extinction coefficient (at 532 nm) with a resolution of 330 m in the horizontal and 30 m in the vertical up to the middle troposphere (Winker et al., 2009). The AERONET network is constituted of sunphotometer instruments measuring a large number of parameters characterizing aerosol population such as AOT, SSA, asymmetry parameter, refractive index and volume size distribution for the whole atmospheric column (Holben et al., 1998). Level 2.0 (cloud free and manually checked) data at 340, 440, 675, 870 and 1020 nm for the station of Moscow (37.30° E and 55.42° N, see Fig. 1) have been used. The uncertainties in AERONET measurements are ± 0.01 for AOT and ± 0.03 for SSA when AOT (440 nm) is larger than 0.2 (Dubovik et al., 2000).

The meteorological conditions over Central Russia during the first part of August 2010 were characterized by persistent dry anticyclonic conditions and high temperatures favourable to the development of intensive wildfires reaching a maximum during the second week of August (Witte et al., 2011). The exceptional nature of this specific episode in terms of particulate pollution can be seen in Fig. 1 showing the spatial distribution of the AOT retrieved by the POLDER sensor (at 550 nm) and modelled by

Fire radiative impacts

J. C. Péré et al.

Title Page

Abstract

Introduction

Conclusions

References

Tables

Figures

◀

▶

◀

▶

Back

Close

Full Screen / Esc

Printer-friendly Version

Interactive Discussion



CHIMERE (at 400 nm) over Eastern Europe from 5 to 12 August 2010 (no data is available for the 8 and 11 August 2010). It should be noted that large areas with no POLDER measurements (white pixels) are present during the period due to cloud contamination. The POLDER cloud-screen algorithm (Bréon and Colzy, 1999) is sometimes too stringent but ensures that the retrieved aerosol properties are not biased by the presence of cloudy structures potentially embedded in the aerosol plume. The satellite observations clearly illustrate both the wide spatial extent and the intensity of the aerosol plume with AOT values (at 550 nm) above 1 over large areas. AOT (550 nm) peaks above 2 are shown as the aerosol plume is transported in an anticyclonic flow from the source region (east of Moscow) to Moscow (6–7 August), towards the north (on 9 August) and back to the east on 10–12 August. The model is able to rather well reproduce the AOT spatial features associated to the transport of particles. However, simulated values are shown to be sometimes underestimated into the advected plume (6, 10 August) and overestimated near the source region (5, 10, 12 August), compared to POLDER measurements. For instance, a clear AOT underestimation occurs over Moscow during the 6 August as the modelled aerosol plume is not enough extended towards the south-west. Over the period, this bias can reach a factor of ± 2 in some areas and can lead to under/over estimate the intensity of the aerosol direct radiative forcing. The injection height of aerosols into the atmosphere is a key parameter controlling the transport and dilution of smoke particles. In our study, it is parametrized based on atmospheric conditions and fire characteristics (such as fire size and flaming intensity) retrieved from MODIS measurements, according to the methodology developed by Hodzic et al. (2007). This estimation can be, however, affected by uncertainties on satellite data. Empirical estimation of the fire injection height is commonly used in meso-scale chemistry-transport models and is generally shown to give a satisfactory representation of fire dynamics (Konovalov et al., 2011; Martins et al., 2012; Fu et al., 2012). Note that some alternative modelling approaches have been recently developed in which the interaction of the atmosphere and the fire is fully resolved at very fine scale (Filippi et al., 2009; Strada et al., 2012). Note also that new retrieval methods are un-

Fire radiative impacts

J. C. Péré et al.

Title Page

Abstract

Introduction

Conclusions

References

Tables

Figures

◀

▶

◀

▶

Back

Close

Full Screen / Esc

Printer-friendly Version

Interactive Discussion



der development for POLDER that will provide the aerosol optical thickness in cloudy scenes (Waquet et al., 2013) and a detailed model of their properties (such as single scattering albedo and size distribution) over cloud-free land scenes (Dubovik et al., 2011). Such new developments will be a useful tool for both a better evaluation and further improvements (through data assimilation for instance) of aerosol simulation by chemistry-transport model like CHIMERE.

The vertical distribution of aerosols during this specific episode has been also recorded during the 9 August by the CALIOP sensor. Figure 2 presents the vertical profile of the aerosol extinction coefficient (in km^{-1}) retrieved by CALIOP (at 532 nm) and modelled by CHIMERE (at 400 nm) during 9 August at midnight in the north of Moscow (59.9° N, 37.6° E) located within the aerosol plume (see Fig. 1). Particles are shown to be confined within the first five km of the atmospheric layer, as shown in CALIOP measurements. There is a peak in the observed signal of 0.8–1.1 km^{-1} around an altitude of 0.8–1 km which rapidly decreases until an altitude of 1.5 km. Above, measured aerosol extinction remains in the range 0.1–0.35 km^{-1} until an altitude of about 5 km from which it becomes negligible. Except for a lack of CALIOP measurements below 0.6 km, the model are within or close to the uncertainty range of observations even if the model tends to overestimate CALIOP values above an altitude of 2 km. As shown hereafter in Fig. 6a, the solar extinction efficiency of fine aerosols is slightly larger at 400 nm than at 532 nm and could partly explain this overestimation. Another reason could be some uncertainties in modelling the release height and dilution of particles in the atmosphere, as previously discussed.

Particulate solar absorption is another important factor in determining the value and sign of the direct radiative forcing of aerosols. The spatial distribution of the daily mean SSA (at 400 nm) between 5 and 12 August 2010 with corresponding AERONET observations (at 440 nm) over Moscow (when available) are presented in Fig. 3. Elevated SSA between 0.93 and 0.97 (at 400 nm) are simulated all along the period over a large part of Eastern Europe, except for a small area in the south-eastern part of the domain where values decrease to 0.89–0.90 during 8 and 9 August 2010. It is interest-

Fire radiative impacts

J. C. Péré et al.

Title Page

Abstract

Introduction

Conclusions

References

Tables

Figures

◀

▶

◀

▶

Back

Close

Full Screen / Esc

Printer-friendly Version

Interactive Discussion



ing to note that no optical signature of the aerosol plume is found in term of aerosol solar absorption compared to the AOT simulation (see Fig. 1). For example, a quite constant SSA of 0.96–0.98 (at 400 nm) is modelled at Moscow before (5–6 August), during (7–10 August) and after (11–12 August) the advection of the aerosol plume over the city, denoting the predominance of scattering species over the period. Such a model behaviour is consistent with corresponding AERONET observations with retrieved SSA values of 0.95–0.96 (at 440 nm) during 7, 10 and 12 August (Fig. 3). This temporal homogeneity of the SSA over the Moscow region can be explained by the analyse of the chemical composition of particles. Figure 4 shows the daily mean percent contribution of the different chemical species to the total PM₁₀ concentration at the surface, modelled at Moscow for each day of the studied period. No clear changes in the aerosol chemical composition are modelled when the aerosol plume overpasses Moscow (7–10 August) compared to the days before (5–6 August) and after (11–12 August), with a predominance of dust and primary (OC) and secondary (SOA) organic carbon, which are considered as mainly scattering in our simulations (see Table 1). The modelled dust, typically made up of resuspended wind-blown particles, is also present in moderate quantity (fraction of 6–13 %) as its emission is favoured by dry soil conditions and fire dynamics. In term of proportion, organics are the dominant part of the aerosol throughout the period with relative contributions of 8–67 % and 16.5–75 % for, respectively, OC and SOA. OC is the major chemical specie between 5 and 10 August (43–67 %) while it is SOA at the end of the period (71–75 %) when the aerosol plume moves away from Moscow. These elevated proportions of organic carbon are the result of large OC and VOC emissions (wildfires + anthropogenic) combined with an important photochemistry favoured by persistent sunny conditions. The other chemical species (SO₄²⁻, NO₃⁻, NH₄⁺, BC, sea salt, water content) are present in lower fraction (0.02–8 %) including black carbon (0.35–0.80 %), which is the main absorbing specie (see refractive index of different particles in Table 1). The important contribution of scattering aerosols results then in elevated values of SSA modelled over Moscow throughout the period. It should also be noted from Fig. 4 that this intense biomass burning

Fire radiative impacts

J. C. Péré et al.

Title Page

Abstract

Introduction

Conclusions

References

Tables

Figures

◀

▶

◀

▶

Back

Close

Full Screen / Esc

Printer-friendly Version

Interactive Discussion



episode is associated to elevated near-surface PM_{10} concentrations over Moscow with daily mean modelled values in the range $100\text{--}300\ \mu\text{g m}^{-3}$ between 6 and 10 August. This estimation is nevertheless lower than the increase of ground particulate pollution observed over this area during the peak of fire event by Konovalov et al. (2011) ($100\text{--}700\ \mu\text{g m}^{-3}$ in daily average).

Compared to SSA, the advection of the aerosol plume over the Moscow region has been clearly detected in the routine measurements of AOT of the corresponding AERONET station. Figure 5 shows the temporal evolution of the daily mean AOT over Moscow retrieved by AERONET (at 340 nm) and modelled by CHIMERE (at 300 nm) between 5 and 12 August 2010. In this figure, we can see an important increase of AERONET AOT from a moderate value of 0.7 on 5 August to very elevated values of 2–4 between 6 and 10 August when the intense aerosol plume overpasses Moscow. Then, moderate AOT (340 nm) of 0.5–0.8 are measured on 11–12 August when the plume moves towards the north and the east (see Fig. 1). The model performs relatively well in simulating the temporal evolution of the observed AOT over this region with biases ranging from -40 to 30% along the period, except for the 6 and 10 August where discrepancy between simulated and observed values is larger due to some uncertainties in simulating the transport of the aerosol plume over Moscow (see Fig. 1).

In a second time, we investigated the spectral evolution of the aerosol optical properties. Figure 6 compares the wavelength dependence of the AOT (averaged between 5 and 12 August) modelled by CHIMERE with corresponding observations at the Moscow AERONET station. Values of modelled and observed Angström exponent are also indicated in parenthesis. In average over the period, the modelled AOT decreases from 1.60 at 300 nm to 0.28 at 1000 nm, which is in accordance with photometric observations. Such a model behaviour is corroborated by good agreement between simulated (1.45) and measured (1.50) Angström exponent indicating that CHIMERE is able to reproduce the fine size mode of particles, as displayed in Fig. 6b. This figure presents the period-averaged column volume size distribution (in $\mu\text{m}^3 \cdot \mu\text{m}^{-2}$) retrieved by AERONET over Moscow and modelled by CHIMERE for the total aerosol popula-

Fire radiative impacts

J. C. Péré et al.

Title Page

Abstract

Introduction

Conclusions

References

Tables

Figures

◀

▶

◀

▶

Back

Close

Full Screen / Esc

Printer-friendly Version

Interactive Discussion



tion and for each chemical components. For the total aerosol distribution, two modes in the accumulation ($r \simeq 0.1\text{--}0.3\ \mu\text{m}$) and coarse size range ($r \geq 1\ \mu\text{m}$) are modelled. This fits well with AERONET retrievals (observed fine mode for radius about $0.2\text{--}0.4\ \mu\text{m}$), although the model simulates a higher volume concentration of very fine particles. In parallel, the coarse mode size distribution is shown to be underestimated by CHIMERE for aerosol radius above $2\ \mu\text{m}$. It should be noted from Fig. 6b that scattering organic aerosols account for a large proportion of the fine mode of particles while the respective contribution of absorbing black carbon is low, as previously seen in Fig. 4. Also, the contribution of scattering resuspended dust in the coarse mode is non-negligible, although under-estimated compared to AERONET. As a consequence, elevated SSA are simulated with a mean value of 0.97 along the $300\text{--}1000\ \text{nm}$ spectral range (Fig. 6c). The low absorbing efficiency of particles associated to a weak spectral dependence are consistent with AERONET observations with values of $0.95\text{--}0.96$ between $440\ \text{nm}$ and $1020\ \text{nm}$. Such aerosol scattering characteristics have been shown to be typical of intense fire conditions previously encountered over Russia (Chubarova et al., 2012).

In summary, the evaluation of the aerosol simulation during this specific episode shows the ability of the model to describe the evolution of the aerosol plume at regional and vertical scale. In addition, CHIMERE is shown to give an appropriate representation of the aerosol size distribution and its extinction and absorbing properties; which is the pre-requisite to study its direct radiative effect and climate feedbacks.

3.2 Direct radiative effect of the aerosol plume and its feedback on air temperature and atmospheric dynamics

Simulated spectral AOT, SSA and g are used to evaluate the impact of particles on shortwave radiative fluxes. Results for the diurnal-averaged ADRF simulated at the ground (ΔF_{BOA}) between 5 and 12 August 2010 over Eastern Europe is displayed in Fig. 7. During the studied period, particles exert an important impact on the energy radiation budget. The shortwave ADRF at the surface is negative over the entire domain with values of -10 to $-150\ \text{W m}^{-2}$ in diurnal-averaged. The surface ADRF spatial

Fire radiative impacts

J. C. Péré et al.

Title Page

Abstract

Introduction

Conclusions

References

Tables

Figures

◀

▶

◀

▶

Back

Close

Full Screen / Esc

Printer-friendly Version

Interactive Discussion



patterns closely follow the AOT spatial pattern. Hence, a maximum reduction of solar energy reaching the ground of $80\text{--}150\text{ W m}^{-2}$ are modelled along the aerosol plume transport. As a consequence, the Moscow region has been subjected to an important aerosol surface forcing, especially during the arrival of the aerosol plume between 6 and 10 August ($40\text{--}90\text{ W m}^{-2}$), which lead to an important impact on the local air temperature profile and atmospheric dynamics. This point will be discussed hereafter in further details. At a regional scale, Fig. 8 indicates that the impact of this shortwave ADRF on the simulated near-surface air temperature is non negligible with a reduction from 0.2 to 2.6°C (in diurnal-averaged) over a large part of the domain. Again, the maximum decrease of air temperature ($1.0\text{--}2.6^\circ$) is shown to be associated with the aerosol plume transport. It is noteworthy from Fig. 8 that the aerosol impact on 2 m temperature is not always correlated to the respective pattern of the surface ADRF (Fig. 7). For example, the decrease of the near-surface air temperature over western Moscow during 8 August ($1.8\text{--}2.2^\circ$) associated to an important surface ADRF ($90\text{--}110\text{ W m}^{-2}$) is similar to the decrease of temperature simulated over the same area during 10 August ($1.6\text{--}2.0^\circ$) for a surface radiative forcing much lower ($30\text{--}60\text{ W m}^{-2}$). Near-surface air temperature mainly depends on incident solar flux, sensible and latent heat fluxes emitted by the terrestrial surface, aerosol solar absorption near the ground and atmospheric circulation. Hence, the resulting effect of these different mechanisms on the 2 m temperature can vary from a region to another, as previously shown by Zaninis (2009) and Péré et al. (2011) over Europe. In turn, this reduction of air temperature due to the presence of aerosols may disturb the atmospheric dynamics such as the development of the atmospheric boundary layer. To further investigate these points, we will now focus our study over the Moscow region, where the surface ADRF and its impact on near-surface air temperature are shown to be pronounced, especially during the aerosol plume overpass (see Figs. 7 and 8).

In Fig. 9a are reported the diurnal-averaged shortwave ADRF (in W m^{-2}) over Moscow simulated at the ground (ΔF_{BOA}) and within the atmosphere (ΔF_{ATM} = difference between the ADRF at the top of the atmosphere and at surface), for each day

Fire radiative impacts

J. C. Péré et al.

Title Page

Abstract

Introduction

Conclusions

References

Tables

Figures

◀

▶

◀

▶

Back

Close

Full Screen / Esc

Printer-friendly Version

Interactive Discussion



of the studied period. We can see that the presence of aerosols reduces significantly the solar energy reaching the surface, especially between 6 and 10 August when the smoke plume is transported towards Moscow (modeled AOT (340 nm) = 1–3.5, see Fig. 5). The maximum reduction occurs on 7, 8 and 9 August when the smoke plume is at its maximum of intensity with diurnal mean ΔF_{BOA} of 65–85 W m⁻², which represents a decrease of about 20–25 % (in average over daytime) of the total shortwave flux at the ground. Such values are comparable (although less pronounced) to the loss of surface shortwave irradiance (30–40 % for AOT(500 nm) = 2–4) inferred from radiative flux measurements over Moscow during this period (Chubarova et al., 2012). The difference may be due to the AOT underestimation, especially during the 7 August. Concerning the ADRF within the atmosphere (ΔF_{ATM}) that represents the amount of solar radiation absorbed by particles in the atmospheric layer, modelled mean values vary from 5 W m⁻² to 26 W m⁻² and accounts only for about 20–30 % of the total simulated ADRF. This moderate proportion of solar absorption by particles is the consequence of their very high scattering efficiency (modelled SSA of 0.97 between 300 and 1000 nm, see Fig. 6c). As previously shown over the entire domain, this important ADRF over Moscow is found to have feedbacks on meteorological parameters such as air temperature. Figure 9b presents the temporal evolution of the 2 m-temperature (averaged over daytime) simulated with and without aerosols along with corresponding observed values. As we can see, the presence of aerosols induces a non-negligible decrease of the near-surface air temperature ranging from 0.5 to 1.6 °C. The highest reduction occurs again on 7, 8 and 9 August when the ADRF is the most pronounced. Compared to the observations, the modelled temperature tends to be overestimated throughout the period, especially when the feedback of the ADRF is not included in the simulation. This result is interesting as WRF is usually known to have a cold bias during the summer season over Europe (Menut et al., 2012), which strengthens the assumption that the ADRF due to the intense aerosol plume could have a regional influence on the air temperature. Indeed, the biases are shown to be clearly reduced when taking into account the aerosol solar extinction, even if a positive bias between simulation

Fire radiative impacts

J. C. Péré et al.

Title Page

Abstract

Introduction

Conclusions

References

Tables

Figures

◀

▶

◀

▶

Back

Close

Full Screen / Esc

Printer-friendly Version

Interactive Discussion



and observations still remains. As illustrated in Fig. 9c, the feedback of the shortwave ADRF does not only occur near the surface but also in the boundary layer. For example, during the 7, 8 and 9 August, the aerosol cooling effect is maximum near the ground (1.2–1.6 °C) and then gradually decreases and becomes negligible from an altitude of about 4000 m where the aerosol solar extinction is low (see Fig. 2). Such vertical structure of air temperature anomaly is favourable to a stabilizing effect in the atmospheric boundary layer (ABL). Indeed, it is clearly shown in Fig. 10a, displaying the temporal evolution of the ABL height during 8 August simulated with and without aerosols, that the radiative effect of particles reduces the development of the boundary layer. For example, a maximum development of 3250 and 3750 m is modelled at midday for, respectively, the simulation with and without aerosols. This result is comparable to the maximum ABL reduction of 800 m (for an AOT(500 nm) = 4) simulated with the on-line WRF-CMAQ model during the June 2008 Californian wildfires (Wong et al., 2012). Using the on-line WRF/Chem-MADRID model, Zhang et al. (2013) modelled a respective change of –40 m (in average over July 2001) corresponding to a mean AOT(600 nm) of 0.6 over the eastern part of Europe. Our simulations indicate that, during daytime, the decrease of the ABL height due to the feedback of the ADRF is comprised between 13 and 65 %. As a consequence, the collapse of the ABL in presence of aerosols occurs one hour earlier (between 14 and 15 h) compared to the simulation without aerosols (between 15 and 16 h). Such weakening of the ABL development is the result of a lower air entrainment, as the vertical wind speed in the ABL is shown to be reduced by 5 to 80 % (at midday) during 8 August when the feedback of the ADRF is taken into account (Fig. 10b).

In turn, this modification of the meteorological parameters due to the feedback of the ADRF could have some potential consequence on the surface air quality. To investigate this point, we have used the WRF meteorological fields including the ADRF feedback as inputs in CHIMERE to re-perform chemistry-transport simulation. Table 3 presents the averaged near-surface concentrations (in $\mu\text{g m}^{-3}$) of PM₁₀, BC, OC, SOA and Dust along with AOT (340 nm) modeled at Moscow for the period 5–12 August 2010, without

Fire radiative impacts

J. C. Péré et al.

Title Page

Abstract

Introduction

Conclusions

References

Tables

Figures

◀

▶

◀

▶

Back

Close

Full Screen / Esc

Printer-friendly Version

Interactive Discussion



the spectral and temporal evolution of aerosol properties at the Moscow AERONET station have been well captured by the model. Observations indicated an important increase of AERONET AOT (340 nm) from 0.7 on 5 August to 2–4 between 6 and 10 August when the aerosol plume was transported over Moscow. The model performed relatively well in simulating the temporal evolution of the observed AOT with biases ranging from –40 to 30 % along the studied period (except for the 6 and 10 August where biases were larger). CHIMERE was able to reproduce the aerosol volume size distribution retrieved by AERONET, leading to good agreement between the modelled and observed wavelength dependence of AOT. Moreover, the model was shown to reproduce the low absorbing efficiency of the aerosol plume (dominated by primary organic species) with modelled elevated SSA (0.97 between 300 and 1000 nm) close to AERONET values over Moscow (0.95–0.96 between 440 and 1020 nm). In a second time, modelled aerosol optical properties have been used in WRF to investigate their direct radiative impacts. During this major fire event, important shortwave aerosol direct radiative forcing have been simulated at the surface ($-(10-150) \text{ W m}^{-2}$ in diurnal-averaged) throughout Eastern Europe. Maximum ADRF values of -80 to -150 W m^{-2} have been obtained over areas under the influence of the aerosol plume. At a regional scale, the impact of this shortwave ADRF on the simulated near-surface air temperature was non negligible with a reduction from 0.2 to 2.6 °C (in diurnal-averaged) over a large part of the domain. Moscow has been also subjected to an important aerosol radiative effect, especially during the arrival of the aerosol plume between 6 and 10 August. Simulations indicated that the presence of the aerosol plume over this area caused a significant reduction of shortwave solar radiation reaching the surface (up to $70-84 \text{ W m}^{-2}$ in diurnal-averaged) with a small part (20–30 %) due to solar absorption within the atmospheric layer. Including the feedback of the ADRF induced a decrease of the near-surface air temperature ranging from 0.5 to 1.6 °C (in diurnal-averaged) and lead to a better agreement with observations. This aerosol cooling effect have been shown to occur over whole the boundary layer and contribute to stabilize it with a reduction of the ABL height in presence of aerosols of 13 to 65 % during daytime. This

Fire radiative impacts

J. C. Péré et al.

[Title Page](#)[Abstract](#)[Introduction](#)[Conclusions](#)[References](#)[Tables](#)[Figures](#)[◀](#)[▶](#)[◀](#)[▶](#)[Back](#)[Close](#)[Full Screen / Esc](#)[Printer-friendly Version](#)[Interactive Discussion](#)

decrease was the result of a lower air entrainment as the vertical wind speed in the ABL was shown to be reduced by 5 to 80 % (at midday) when the feedback of the ADRF is taken into account, with some consequence on the surface particulate pollution. Indeed, a CHIMERE sensitivity test, driven by the WRF meteorological fields including the ADRF feedback, predicted a large increase in the near-surface PM_{10} concentrations (up to 99 %) due to the lower vertical dilution. As a result, biases with the PM_{10} concentrations observed over Moscow during this specific period have been reduced. However, the aerosol direct radiative effect on ABL ventilation is not the only factor that could influence particulate pollution. Alteration of photolysis rates by the aerosol solar extinction could affect the formation of secondary species and hence the concentration of particles. This last point will be investigated in a future study by using a complete on-line coupling between CHIMERE and the Tropospheric Ultraviolet and Visible radiation model.

Acknowledgements. Authors are grateful to the CRI at Lille 1 for its technical support. This work was partly funded by the french ministry in charge of Ecology and the PRIMEQUAL program (APIFLAME). We also acknowledge the University of Wyoming for providing us the meteorological data. Anthony Ung (INERIS) is acknowledged for his help in processing the fire emissions data.



The publication of this article is financed by CNRS-INSU.

References

Bessagnet, B., Hodzic, A., Vautard, R., Beekmann, M., Cheinet, S., Honoré, C., Liousse, C., and Rouil, L.: Aerosol modeling with CHIMERE–Preliminary evaluation at the continental scale, *Atmos. Environ.*, 38, 2803–2817, 2004. 15834

Fire radiative impacts

J. C. Péré et al.

Title Page

Abstract

Introduction

Conclusions

References

Tables

Figures

◀

▶

◀

▶

Back

Close

Full Screen / Esc

Printer-friendly Version

Interactive Discussion



- Bessagnet, B., Menut, L., Curci, G., Hodzic, A., Guillaume, B., Lioussé, C., Moukhtar, S., Pun, B., Seigneur, C., and Schulz, M.: Regional modeling of carbonaceous aerosols over Europe – focus on secondary organic aerosols, *J. Atmos. Chem.*, 61, 175–202, 2009. 15834
- Bréon, F. M. and Colzy, S.: Cloud detection from the spaceborne POLDER instrument and validation against surface synoptic observations, *J. Appl. Meteorol.*, 36, 777–785, 1999. 15838
- Carlsaw, K. S., Boucher, O., Spracklen, D. V., Mann, G. W., Rae, J. G. L., Woodward, S., and Kulmala, M.: A review of natural aerosol interactions and feedbacks within the Earth system, *Atmos. Chem. Phys.*, 10, 1701–1737, doi:10.5194/acp-10-1701-2010, 2010. 15832
- Chen, F. and Dudhia, J.: Coupling an advanced land-surface/hydrology model with the Penn State/NCAR MM5 modeling system. Part 1: Model description and implementation, *Mon. Weather Rev.*, 129, 569–585, 2001. 15835
- Chou, M. D. and Suarez, M. J.: An efficient thermal infrared radiation parametrization for use in general circulation models, NASA, Tech. Memo., 3, tM-104606, 85 pp., USA NASA technical report series on global modeling and data assimilation, 1994. 15836
- Chubarova, N., Nezval', Ye., Sviridenkov, I., Smirnov, A., and Slutsker, I.: Smoke aerosol and its radiative effects during extreme fire event over Central Russia in summer 2010, *Atmos. Meas. Tech.*, 5, 557–568, doi:10.5194/amt-5-557-2012, 2012. 15833, 15842, 15844
- d'Almeida, G. A., Koepke, P., and Shettle, E. P.: Atmospheric aerosols: Global climatology and radiative characteristics, A. Deepak, Hampton, Va, 1991. 15854
- Deuzé, J. L., Bréon, F. M., Devaux, C., Goloub, P., Herman, M., Lafrance, B., Maignan, F., Marchand, A., Nadal, F., Perry, G., and Tanré, D.: Remote sensing of aerosols over land surface from POLDER-ADEOS-1 polarized measurements, *J. Geophys. Res.*, 106, 4913–4926, 2001. 15837
- Dubovik, O., Smirnov, A., Holben, B., King, M., Kaufman, Y., Eck, T., and Slutsker, I.: Accuracy assessments of aerosol optical properties retrieved from Aerosol Robotic Network (AERONET) Sun and sky radiance measurements, *J. Geophys. Res.*, 105, 9791–9806, 2000. 15837, 15861, 15862
- Dubovik, O., Herman, M., Holdak, A., Lapyonok, T., Tanré, D., Deuzé, J. L., Ducos, F., Sinyuk, A., and Lopatin, A.: Statistically optimized inversion algorithm for enhanced retrieval of aerosol properties from spectral multi-angle polarimetric satellite observations, *Atmos. Meas. Tech.*, 4, 975–1018, doi:10.5194/amt-4-975-2011, 2011. 15839

Fire radiative impacts

J. C. Péré et al.

Title Page

Abstract

Introduction

Conclusions

References

Tables

Figures

◀

▶

◀

▶

Back

Close

Full Screen / Esc

Printer-friendly Version

Interactive Discussion



- Filippi, J. B., Bosseur, F., Mari, C., Lac, C., Moigne, P. L., Cuenot, B., Veynante, D., Cariolle, D., and Balbi, J. H.: Coupled atmosphere–wildland fire modelling, *J. Adv. Model. Earth Syst.*, 1, 11, 9 pp., doi:10.3894/JAMES.2009.1.11, 2009. 15838
- 5 Forster, P., Ramaswamy, V., Artaxo, P., Bernsten, T., Betts, R., Fahey, D. W., Haywood, J., Lean, J., Lowe, D. C., Myhre, G., Nganga, J., Prinn, R., Raga, G., Schulz, M., and Dorland, R. V.: Changes in atmospheric constituents and in radiative forcing, in: *Climate Change 2007: The Physical Science Basis, Contribution of Working Group I to the Fourth Assessment Report of the Intergovernmental Panel on Climate Change*, edited by: Solomon, S., Qin, D., Manning, M., Chen, Z., Marquis, M., Averyt, K. B., Tignor, M., and Miller, H. L., IPCC report, Cambridge University Press, Cambridge, United Kingdom and New York, NY, USA, 2007. 15832
- 10 Fu, J. S., Hsu, N. C., Gao, Y., Huang, K., Li, C., Lin, N.-H., and Tsay, S.-C.: Evaluating the influences of biomass burning during 2006 BASE-ASIA: a regional chemical transport modeling, *Atmos. Chem. Phys.*, 12, 3837–3855, doi:10.5194/acp-12-3837-2012, 2012. 15838
- 15 Guenther, A., Karl, T., Harley, P., Wiedinmyer, C., Palmer, P. I., and Geron, C.: Estimates of global terrestrial isoprene emissions using MEGAN (Model of Emissions of Gases and Aerosols from Nature), *Atmos. Chem. Phys.*, 6, 3181–3210, doi:10.5194/acp-6-3181-2006, 2006. 15834
- Hess, M., Koepke, P., and Schult, I.: Optical properties of aerosols and clouds: the software package OPAC, *B. Am. Meteorol. Soc.*, 79, 831–844, 1998. 15836, 15855
- 20 Hodzic, A., Madronich, S., Bohn, B., Massie, S., Menut, L., and Wiedinmyer, C.: Wildfire particulate matter in Europe during summer 2003: meso-scale modeling of smoke emissions, transport and radiative effects, *Atmos. Chem. Phys.*, 7, 4043–4064, doi:10.5194/acp-7-4043-2007, 2007. 15838
- 25 Holben, B., Eck, T., Slutsker, I., Tanré, D., Buis, J., Setzer, A., Vermote, E., Reagan, J., Kaufman, Y., Nakajima, T., Lavenu, F., Jankowiak, I., and Smirnov, A.: AERONET: a federated instrument network and data archive for aerosol characterization, *Remote Sens. Environ.*, 66, 1–16, 1998. 15837
- Hong, S. Y.: Stable boundary layer mixing in a vertical diffusion scheme, paper presented at the Korea Meteorological Society fall conference Seoul, 25–26 October, 2007. 15835
- 30 Hong, S. Y., Noh, Y., and Dudhia, J.: A new vertical diffusion package with an explicit treatment of entrainment processes, *Mon. Weather Rev.*, 134, 2318–2341, 2006. 15835

Fire radiative impacts

J. C. Péré et al.

Title Page

Abstract

Introduction

Conclusions

References

Tables

Figures

I◀

▶I

◀

▶

Back

Close

Full Screen / Esc

Printer-friendly Version

Interactive Discussion



Junker, C. and Lioussé, C.: A global emission inventory of carbonaceous aerosol from historic records of fossil fuel and biofuel consumption for the period 1860–1997, *Atmos. Chem. Phys.*, 8, 1195–1207, doi:10.5194/acp-8-1195-2008, 2008. 15834

5 Kain, J. S.: The Kain–Fritsch convective parametrization: an update, *J. Appl. Meteorol.*, 43, 170–181, 2004. 15835

Kaiser, J. W., Heil, A., Andreae, M. O., Benedetti, A., Chubarova, N., Jones, L., Morcrette, J.-J., Razinger, M., Schultz, M. G., Suttie, M., and van der Werf, G. R.: Biomass burning emissions estimated with a global fire assimilation system based on observed fire radiative power, *Biogeosciences*, 9, 527–554, doi:10.5194/bg-9-527-2012, 2012. 15834, 15835

10 Konovalov, I. B., Beekmann, M., Kuznetsova, I. N., Yurova, A., and Zvyagintsev, A. M.: Atmospheric impacts of the 2010 Russian wildfires: integrating modelling and measurements of an extreme air pollution episode in the Moscow region, *Atmos. Chem. Phys.*, 11, 10031–10056, doi:10.5194/acp-11-10031-2011, 2011. 15833, 15838, 15841, 15846

Krekov, G. M.: *Aerosols Effects on Climate*, University of Arizona Press, Tucson, 1993. 15854

15 Malavelle, F., Pont, V., Mallet, M., Solmon, F., Johnson, B., Leon, J. F., and Lioussé, C.: Simulation of aerosol radiative effects over West Africa during DABEX and AMMA SOP-0, *J. Geophys. Res.*, 116, D08205, doi:10.1029/2010JD014829, 2011. 15832

20 Marley, N. A., Gaffney, J. S., Baird, J. C., Blazer, C. A., Drayton, P. J., and Frederick, J. E.: An empirical method for the determination of the complex refractive index of size-fractionated atmospheric aerosols for radiative transfer calculations, *Aerosol Sci. Tech.*, 34, 535–549, 2001. 15854

Martins, V., Miranda, A. I., Carvalho, A., Schaap, M., Borrego, C., and Sa, E.: Impact of forest fires on particulate matter and ozone levels during the 2003, 2004 and 2005 fire seasons in Portugal, *Sci. Total. Environ.*, 414, 53–62, 2012. 15838

25 Menut, L., Tripathi, O. M., Colette, A., Vautard, R., Flaounas, E., and Bessagnet, B.: Evaluation of regional climate simulations for air quality modelling purposes, *Clim. Dynam.*, 40, 2515–2533, doi:10.1007/s00382-012-1345-9, 2012. 15844

30 Menut, L., Bessagnet, B., Khvorostyanov, D., Beekmann, M., Colette, A., Coll, I., Curci, G., Foret, G., Hodzic, A., Mailler, S., Meleux, F., Monge, J.-L., Pison, I., Turquety, S., Valari, M., Vautard, R., and Vivanco, M. G.: Regional atmospheric composition modeling with CHIMERE, *Geosci. Model Dev. Discuss.*, 6, 203–329, doi:10.5194/gmdd-6-203-2013, 2013. 15833, 15834

Fire radiative impacts

J. C. Péré et al.

Title Page

Abstract

Introduction

Conclusions

References

Tables

Figures

◀

▶

◀

▶

Back

Close

Full Screen / Esc

Printer-friendly Version

Interactive Discussion



Mlawer, E., Taubman, S., Brown, P., Iacono, M., and Clough, S.: Radiative transfer for inhomogeneous atmospheres: RRTM, a validated correlated-K model for the longwave, *J. Geophys. Res.*, 102, 16633–16682, 1997. 15836

Moritz, M. A., Parisien, M.-A., Battlori, E., Krawchuk, M. A., Dorn, J. V., Ganz, D. J., and Hayhoe, K.: Climate change and disruptions to global fire activity, *Ecosphere*, 3, 49, doi:10.1890/ES11-00345.1, 2012. 15832

Ott, L., Duncan, B., Pawson, S., Colarco, P., Chin, M., Randles, C., Diehl, T., and Nielsen, E.: Influence of the 2006 Indonesian biomass burning aerosols on tropical dynamics studied with the GEOS-5 AGCM, *J. Geophys. Res.*, 115, D14121, doi:10.1029/2009JD013181, 2010. 15832

Péré, J. C., Mallet, M., Bessagnet, B., and Pont, V.: Evidence of the aerosol core-shell mixing state over Europe during the heat wave of summer 2003 by using CHIMERE simulations and AERONET inversions, *Geophys. Res. Lett.*, 36, L09807, doi:10.1029/2009GL037334, 2009. 15835

Péré, J. C., Mallet, M., Pont, V., and Bessagnet, B.: Evaluation of an aerosol optical scheme in the chemistry-transport model CHIMERE, *Atmos. Environ.*, 44, 3688–3699, 2010. 15835

Péré, J. C., Mallet, M., Pont, V., and Bessagnet, B.: Impact of aerosol direct radiative forcing on the radiative budget, surface heat fluxes, and atmospheric dynamics during the heat wave of summer 2003 over western Europe: a modeling study, *J. Geophys. Res.*, 116, D23119, doi:10.1029/2011JD016240, 2011. 15835, 15836, 15843

Pun, B., Seigneur, C., and Lohman, K.: Modeling secondary organic aerosol via multiphase partitioning with molecular data, *Environ. Sci. Technol.*, 40, 4722–4731, 2006. 15834

Skamarock, W. C., Klemp, J. B., and Dudhia, J.: Prototypes for the WRF (Weather Research and Forecasting) model, paper presented at the ninth conference on mesoscale processes, A. M. Meteorol. Soc., Fort Lauderdale, Fla., 2001. 15833, 15835

Strada, S., Mari, C., Filippi, J. B., and Bosseur, F.: Wildfire and the atmosphere: modelling the chemical and dynamic interactions at the regional scale, *Atmos. Environ.*, 51, 234–249, 2012. 15838

Tanré, D., Bréon, F. M., Deuzé, J. L., Dubovik, O., Ducos, F., François, P., Goloub, P., Herman, M., Lifermann, A., and Waquet, F.: Remote sensing of aerosols by using polarized, directional and spectral measurements within the A-Train: the PARASOL mission, *Atmos. Meas. Tech.*, 4, 1383–1395, doi:10.5194/amt-4-1383-2011, 2011. 15837

Fire radiative impacts

J. C. Péré et al.

Title Page

Abstract

Introduction

Conclusions

References

Tables

Figures

◀

▶

◀

▶

Back

Close

Full Screen / Esc

Printer-friendly Version

Interactive Discussion



Tummon, F., Solmon, F., Liousse, C., and Tadross, M.: Simulation of the direct and semidirect aerosol effects on the southern Africa regional climate during the biomass burning season, *J. Geophys. Res.*, 115, D19206, doi:10.1029/2009JD013738, 2011. 15832

Vautard, R., Bessagnet, B., Chin, M., and Menut, L.: On the contribution of natural aeolian sources to particulate matter concentrations in Europe: testing hypotheses with a modelling approach, *Atmos. Environ.*, 39, 3291–3303, 2005. 15834

Waquet, F., Cornet, C., Deuzé, J.-L., Dubovik, O., Ducos, F., Goloub, P., Herman, M., Lapyonok, T., Labonnote, L. C., Riedi, J., Tanré, D., Thieuleux, F., and Vanbauce, C.: Retrieval of aerosol microphysical and optical properties above liquid clouds from POLDER/PARASOL polarization measurements, *Atmos. Meas. Tech.*, 6, 991–1016, doi:10.5194/amt-6-991-2013, 2013 15839

Winker, D. M., Vaughan, M. A., Omar, A., Hu, Y., Powell, K. A., Liu, Z., Hunt, W. H., and Young, S. A.: Overview of the CALIPSO mission and CALIOP data processing algorithms, *J. Atmos. Ocean. Tech.*, 26, 2310–2323, 2009. 15837

Witte, J. C., Douglass, A. R., da Silva, A., Torres, O., Levy, R., and Duncan, B. N.: NASA A-Train and Terra observations of the 2010 Russian wildfires, *Atmos. Chem. Phys.*, 11, 9287–9301, doi:10.5194/acp-11-9287-2011, 2011. 15833, 15837

Wong, D. C., Pleim, J., Mathur, R., Binkowski, F., Otte, T., Gilliam, R., Pouliot, G., Xiu, A., Young, J. O., and Kang, D.: WRF-CMAQ two-way coupled system with aerosol feedback: software development and preliminary results, *Geosci. Model Dev.*, 5, 299–312, doi:10.5194/gmd-5-299-2012, 2012. 15845

Zanis, P.: A study on the direct effect of anthropogenic aerosols on near surface air temperature over Southeastern Europe during summer 2000 based on regional climate modeling, *Ann. Geophys.*, 27, 3977–3988, doi:10.5194/angeo-27-3977-2009, 2009. 15843

Zhang, Y., Fu, R., Yu, H., Qian, Y., Dickinson, R., Dias, M. A. F. S., Dias, P. L. D. S., and Fernandes, K.: Impact of biomass burning aerosol on the monsoon circulation transition over Amazonia, *Geophys. Res. Lett.*, 36, L10814, doi:10.1029/2009GL037180, 2009. 15832

Zhang, Y., Sartelet, K., Zhu, S., Wang, W., Wu, S.-Y., Zhang, X., Wang, K., Tran, P., Seigneur, C., and Wang, Z.-F.: Application of WRF/Chem-MADRID and WRF/Polyphemus in Europe – Part 2: Evaluation of chemical concentrations, sensitivity simulations, and aerosol-meteorology interactions, *Atmos. Chem. Phys. Discuss.*, 13, 4059–4125, doi:10.5194/acpd-13-4059-2013, 2013. 15845

Fire radiative impacts

J. C. Péré et al.

Table 1. Wavelength-dependent complex refractive index of each chemical species used to perform optical calculation. n and k are, respectively, the real and imaginary parts of the complex refractive index.

Species	Complex refractive index ($n - ik$)	
	300–400 nm	600–999 nm
Nitrate ^a	$1.53 - i0.006$	$1.53 - i0.006$
Ammonium ^b	$1.52 - i0.0005$	$1.52 - i0.0005$
Sulphate ^b	$1.44 - i10^{-8}$	$1.43 - i2.6 \times 10^{-8}$
OC ^b	$1.45 - i0.001$	$1.45 - i0.001$
BC ^c	$1.87 - i0.569$	$1.87 - i0.569$
SOA ^b	$1.45 - i0.001$	$1.45 - i0.001$
Sea Salt ^b	$1.45 - i0.0056$	$1.45 - i5 \times 10^{-5}$
Dust ^b	$1.52 - i0.008$	$1.51 - i0.008$
Water ^b	$1.34 - i2 \times 10^{-9}$	$1.33 - i3.4 \times 10^{-8}$

^a See d'Almeida et al. (1991).

^b See Krekov (1993).

^c See Marley et al. (2001).

[Title Page](#)
[Abstract](#)
[Introduction](#)
[Conclusions](#)
[References](#)
[Tables](#)
[Figures](#)
[◀](#)
[▶](#)
[◀](#)
[▶](#)
[Back](#)
[Close](#)
[Full Screen / Esc](#)
[Printer-friendly Version](#)
[Interactive Discussion](#)


Fire radiative impacts

J. C. Péré et al.

Title Page

Abstract

Introduction

Conclusions

References

Tables

Figures

I◀

▶I

◀

▶

Back

Close

Full Screen / Esc

Printer-friendly Version

Interactive Discussion



Table 2. Climatology of aerosol optical properties for the free troposphere and the stratosphere issued from Hess et al. (1998).

	Free troposphere (6–12 km)				Stratosphere (12–20 km)			
	0.3 μm	0.4 μm	0.6 μm	0.99 μm	0.3 μm	0.4 μm	0.6 μm	0.99 μm
AOT	0.025	0.019	0.011	0.006	0.010	0.007	0.005	0.001
SSA	0.94	0.94	0.94	0.94	1	1	1	1
<i>g</i>	0.7	0.7	0.7	0.7	0.7	0.7	0.7	0.7

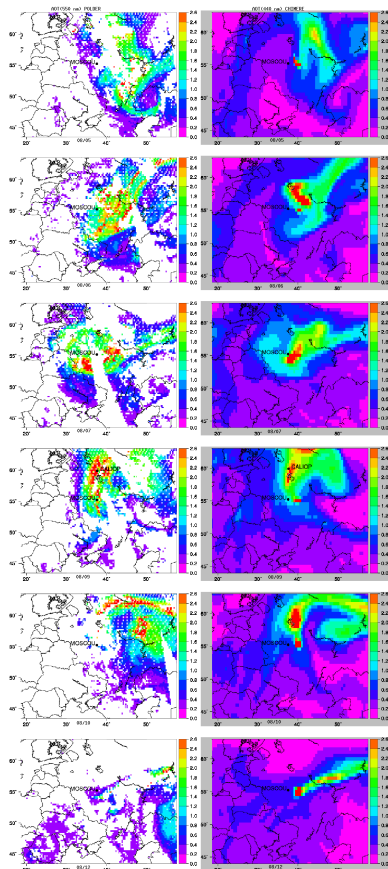


Fig. 1. Geographic distribution of the AOT over Eastern Europe from 5 to 12 August 2010 observed by the POLDER satellite sensor (at 550 nm) and modelled by CHIMERE (at 400 nm). The AERONET station of Moscow and the location of CALIOP measurements analysed in this study are also indicated.

Fire radiative impacts

J. C. Péré et al.

Title Page

Abstract Introduction

Conclusions References

Tables Figures

◀ ▶

◀ ▶

Back Close

Full Screen / Esc

Printer-friendly Version

Interactive Discussion



Fire radiative impacts

J. C. Péré et al.

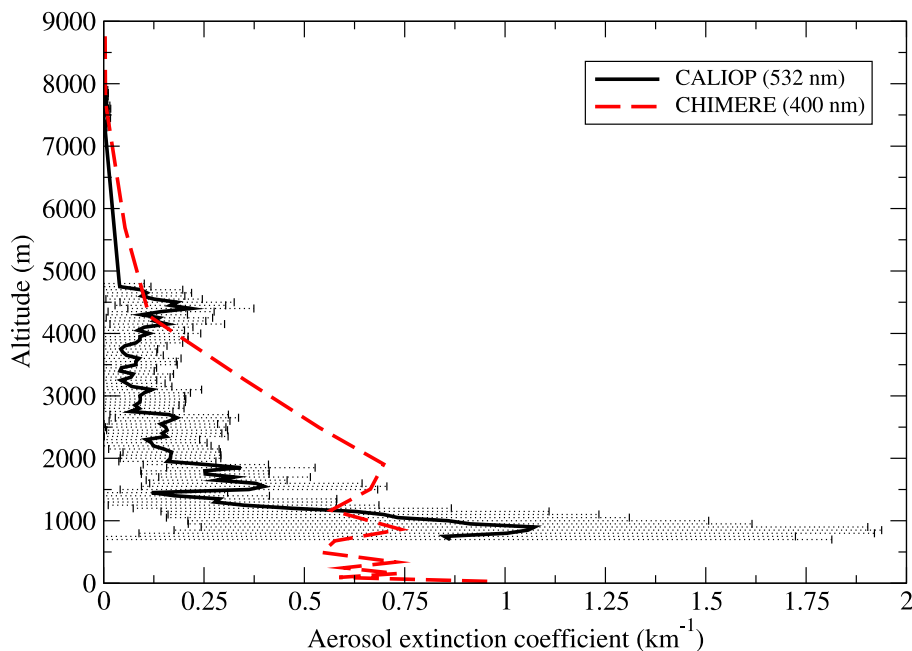


Fig. 2. Vertical profile of the aerosol extinction coefficient (in km^{-1}) retrieved by CALIOP (at 532 nm) and modelled by CHIMERE (at 400 nm) during 9 August at midnight in the north of Moscow (59.9° N, 37.6° E) located within the aerosol plume (see Fig. 1). Uncertainty on CALIOP measurements are also indicated by error bars.

[Title Page](#)[Abstract](#)[Introduction](#)[Conclusions](#)[References](#)[Tables](#)[Figures](#)[◀](#)[▶](#)[◀](#)[▶](#)[Back](#)[Close](#)[Full Screen / Esc](#)[Printer-friendly Version](#)[Interactive Discussion](#)

Fire radiative impacts

J. C. Péré et al.

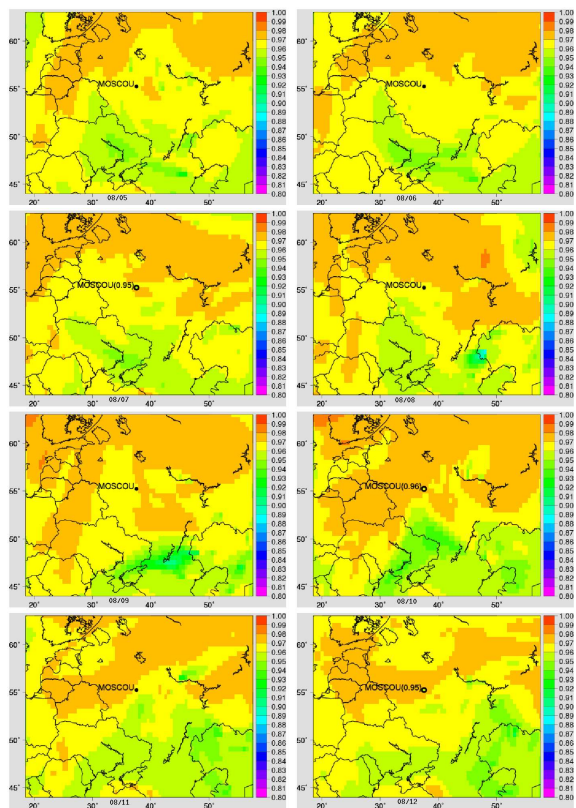


Fig. 3. Geographic distribution of the daily mean SSA over Eastern Europe from 5 to 12 August 2010 modelled by CHIMERE (at 400 nm) and measured at the Moscow AERONET station (at 440 nm) during 7, 10 and 12 August (no data is available for the others days of the studied period).

[Title Page](#)[Abstract](#)[Introduction](#)[Conclusions](#)[References](#)[Tables](#)[Figures](#)[◀](#)[▶](#)[◀](#)[▶](#)[Back](#)[Close](#)[Full Screen / Esc](#)[Printer-friendly Version](#)[Interactive Discussion](#)

Fire radiative impacts

J. C. Péré et al.

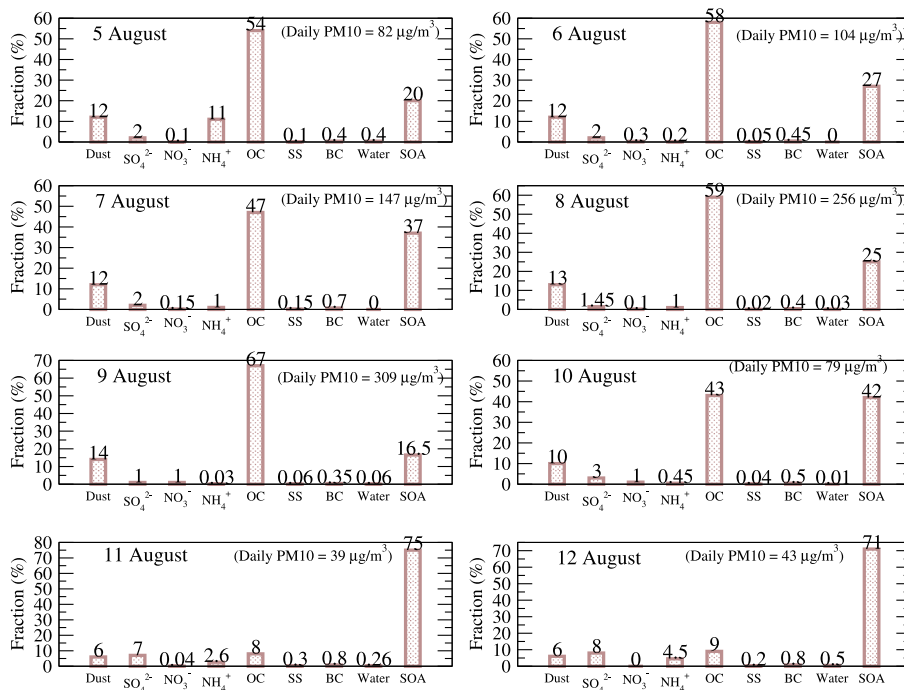


Fig. 4. Daily mean percent distribution of the different chemical species to the total PM₁₀ concentrations at the surface modelled at Moscow for each day of the studied period (SS: Sea Salt). Daily mean values of the total PM₁₀ surface concentrations (in μg m⁻³) are also indicated in parenthesis.

[Title Page](#)
[Abstract](#)
[Introduction](#)
[Conclusions](#)
[References](#)
[Tables](#)
[Figures](#)
[◀](#)
[▶](#)
[◀](#)
[▶](#)
[Back](#)
[Close](#)
[Full Screen / Esc](#)
[Printer-friendly Version](#)
[Interactive Discussion](#)


Fire radiative impacts

J. C. Péré et al.

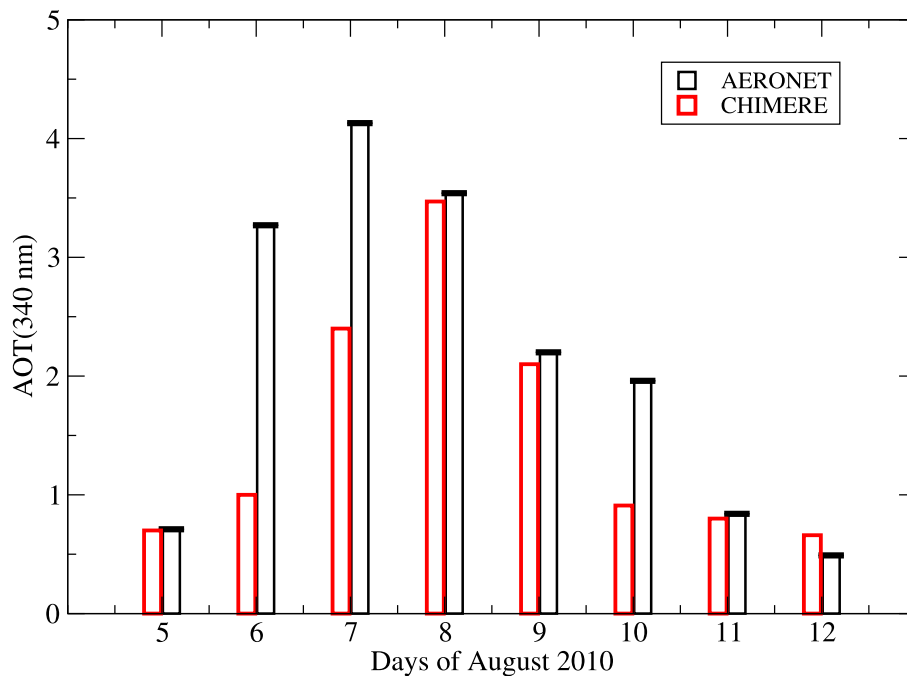


Fig. 5. Temporal evolution of the daily mean observed and modelled AOT(340 nm) over Moscow between 5 and 12 August 2010. Error bars represent the uncertainty range of observations (± 0.01 , see Dubovik et al., 2000).

[Title Page](#)[Abstract](#)[Introduction](#)[Conclusions](#)[References](#)[Tables](#)[Figures](#)[◀](#)[▶](#)[◀](#)[▶](#)[Back](#)[Close](#)[Full Screen / Esc](#)[Printer-friendly Version](#)[Interactive Discussion](#)

Fire radiative impacts

J. C. Péré et al.

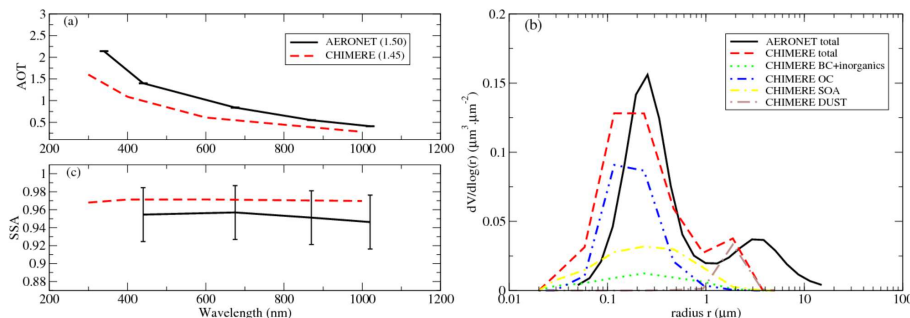


Fig. 6. Wavelength dependence of the **(a)** AOT and **(c)** SSA averaged over 5–12 August 2010 simulated by CHIMERE with corresponding AERONET observations over Moscow. Error bars represent the uncertainty range of observations for SSA (± 0.03 , see Dubovik et al., 2000) and AOT. Values of the observed and modelled Angström exponent are indicated in parenthesis. **(b)** Column volume size distribution retrieved by AERONET and modelled by CHIMERE for the total aerosol population and for each chemical species.

Title Page

Abstract

Introduction

Conclusions

References

Tables

Figures

◀

▶

◀

▶

Back

Close

Full Screen / Esc

Printer-friendly Version

Interactive Discussion



Fire radiative impacts

J. C. Péré et al.

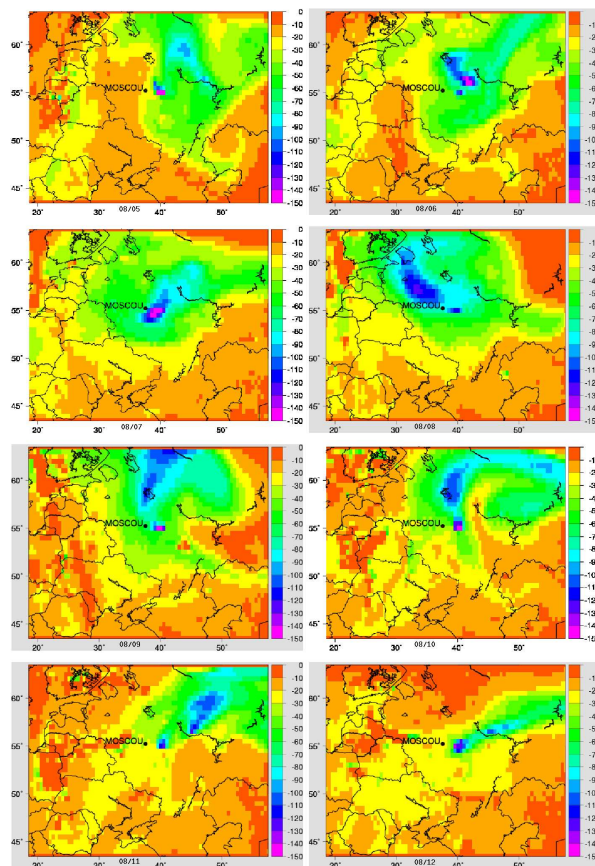


Fig. 7. Geographic distribution of the diurnal-averaged shortwave ADRF (in Wm^{-2}) simulated at the surface between 5 and 12 August 2010.

[Title Page](#)[Abstract](#)[Introduction](#)[Conclusions](#)[References](#)[Tables](#)[Figures](#)[◀](#)[▶](#)[◀](#)[▶](#)[Back](#)[Close](#)[Full Screen / Esc](#)[Printer-friendly Version](#)[Interactive Discussion](#)

Fire radiative impacts

J. C. Péré et al.

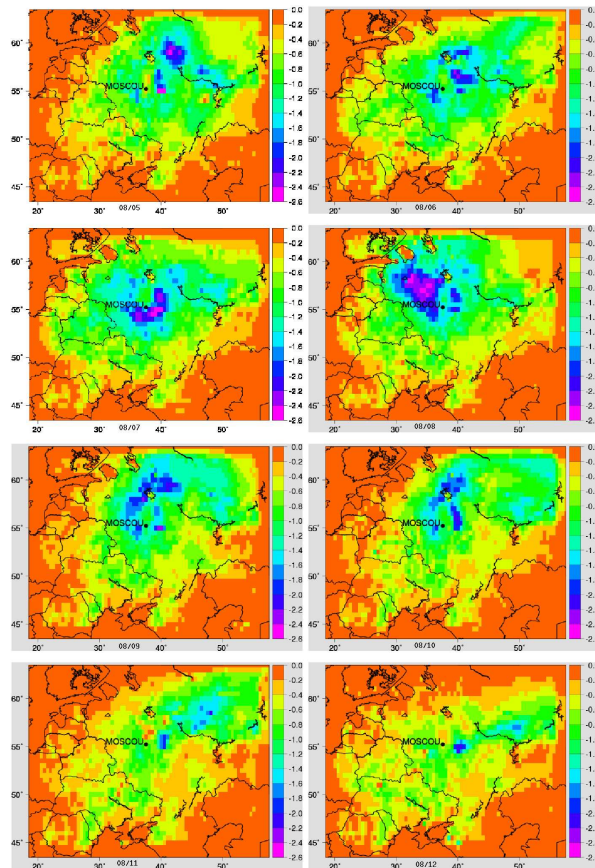


Fig. 8. Impact of the shortwave ADRF on the diurnal-averaged near-surface air temperature (in degrees) simulated between 5 and 12 August 2010.

[Title Page](#)[Abstract](#)[Introduction](#)[Conclusions](#)[References](#)[Tables](#)[Figures](#)[◀](#)[▶](#)[◀](#)[▶](#)[Back](#)[Close](#)[Full Screen / Esc](#)[Printer-friendly Version](#)[Interactive Discussion](#)

Fire radiative impacts

J. C. Péré et al.

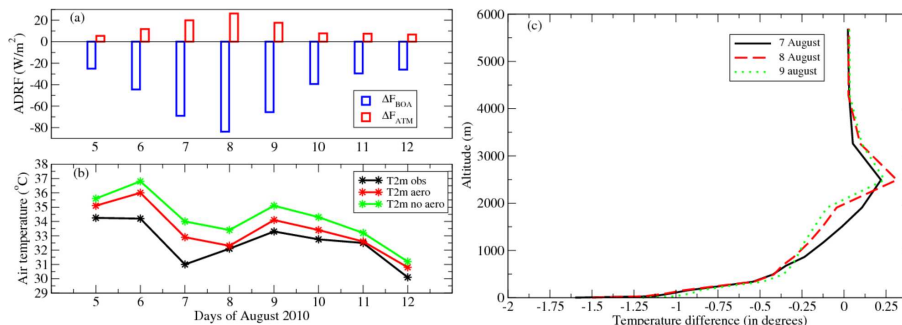


Fig. 9. Diurnal-averaged **(a)** shortwave aerosol direct radiative forcing (in Wm^2) simulated at the surface (ΔF_{BOA}) and within the atmosphere (ΔF_{ATM}) and **(b)** near-surface air temperature (in $^{\circ}\text{C}$) simulated with and without aerosols and observed at the meteorological station of Moscow-Domodedov, for each day of the studied period. **(c)** Impact of the ADRF on the vertical profile of the diurnal-averaged air temperature (in degrees) simulated for the 7 and 8 August 2010 over Moscow.

Fire radiative impacts

J. C. Péré et al.

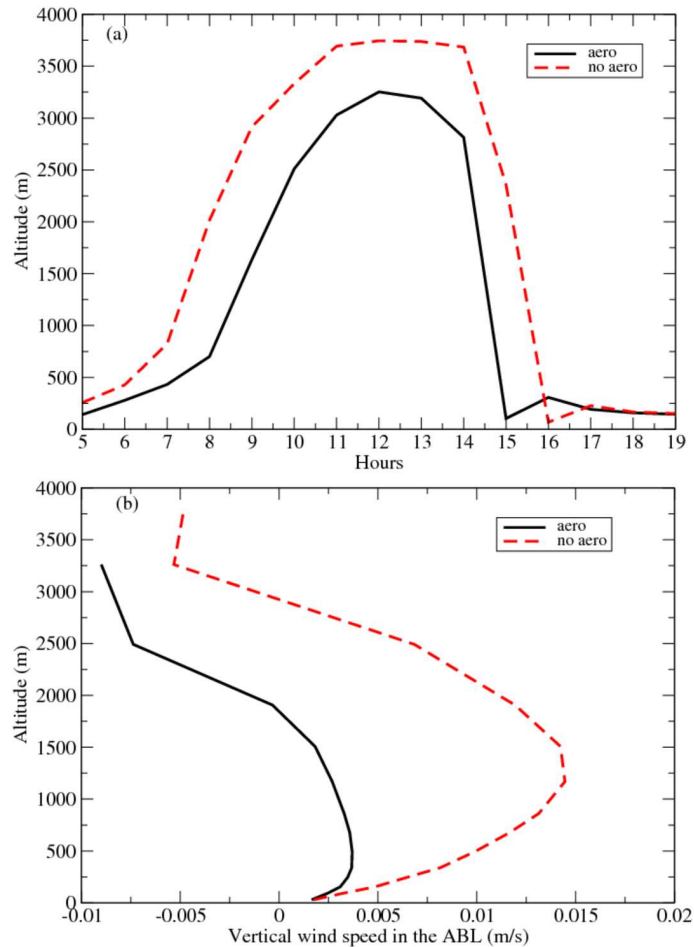


Fig. 10. (a) Temporal evolution of the atmospheric boundary layer (ABL) and (b) vertical wind speed in the ABL at midday, simulated with and without aerosols during 8 August.